Static magnetic properties and relaxation of the insulating spin glass $Co_{1-x}Mn_xCl_2 \cdot H_2O$

G. C. DeFotis, G. S. Coker,* J. W. Jones, C. S. Branch, H. A. King, J. S. Bergman, S. Lee, and J. R. Goodey
Chemistry Department, College of William and Mary, Williamsburg, Virginia 23187
(Received 26 January 1998; revised manuscript received 22 June 1998)

The magnetic properties of $Co_{1-x}Mn_xCl_2 \cdot H_2O$ are examined by dc magnetization and susceptibility measurements, for $x=0.05$, 0.10, 0.20, 0.30, 0.40, 0.50, 0.60, 0.70, 0.80, 0.90, and 0.95 between 1.8 and 300 K. The pure components are a quasi-one-dimensional Heisenberg antiferromagnet (Mn) and an antiferromagnetic reentrant spin glass (Co) with some low-dimensional character. The Curie and Weiss constants, in $\chi_M = C/(T-\theta)$, show regular composition dependence, with $\theta(x)$ varying nonlinearly from positive to negative values as x increases. Antiferromagnetic maxima often occur, and transition temperatures are estimated for most mixtures. The T-x diagram shows two descending boundaries from either composition extreme; any transition temperatures for $x=0.5-0.8$ are lower than we can measure. Magnetization isotherms evolve with composition, and associated hysteretic effects weaken with increasing x. The nonlinear susceptibility for $x=0.30$ shows structure, but does not diverge. The thermoremanent magnetization (TRM) is examined in detail for $x=0.30$, 0.40, and 0.50. Its temperature dependence shows characteristic features, but does not follow any simple form. Systematic variation in the TRM with cooling field and composition is apparent. The time dependence of the TRM is fit using a stretched exponential decay form. Systematic variations in the fit parameters with temperature, cooling field, and composition emerge. For low to moderate temperatures, the TRM is found to scale according to $T\ \log_{10}(t/\tau_0)$, with $\tau_0 \approx 10^{-12}-10^{-13}$ s. For $x=0.30$ and 0.50, strong and weak irreversibility lines are determined. The former conform better to a recent prediction for the short-range three-dimensional Ising spin glass, $\tau_g \propto h^{0.53}$, than to the DeAlmeida-Thouless mean-field form $\tau_g \propto h^{2/3}$; best-fit exponents are slightly less than 0.53. For the weak irreversibility lines, the dependence of τ_g on field is much weaker than the Gabay-Toulouse form $\tau_g \propto h^2$. The presence of strong random anisotropy is a possible explanation. A monotonic decrease of T_s with increasing x is found. A reentrant spin glass state still occurs for $x=0.30$; for $x=0.40$ and 0.50, the spin glass transition is not reentrant. Irreversible effects are maximized in the $x=0.3-0.4$ region; they are absent for mixtures richer in manganese than cobalt. [S0163-1829(98)09341-2]

I. INTRODUCTION

Randomly mixed magnetic systems have been the subject of much study in the past two decades. Mixed systems in which the pure components possess competing orthogonal spin anisotropies were of greatest early interest.[1,2] A very well studied case is $Fe_{1-x}Co_xCl_2$;[3,4] $Fe_{1-x}Co_xBr_2$ has also been examined.[5] We have studied $Fe_{1-x}Mn_xCl_2 \cdot 2H_2O$,[6] which has an especially complex phase diagram due to the presence of competing ferromagnetic and antiferromagnetic exchange interactions and orthogonal anisotropies. The structurally isomorphous dihydrate mixture $Fe_{1-x}Co_xCl_2 \cdot 2H_2O$ is simpler in that competing exchange interactions are absent.[7] Interest in such systems centers mainly on the tetracritical point in the T-composition magnetic phase diagram and on the coupling between spin components ordering at different temperatures.

A second important type of mixed magnet is one in which competing ferromagnetic and antiferromagnetic exchange interactions occur,[8] but without competing spin anisotropies, so that the behavior is mainly determined by exchange frustration effects. Probably the best studied system of this type is $Fe_xMn_{1-x}TiO_3$.[9] An example studied in this laboratory[10] and elsewhere[11] is $Co_{1-x}Mn_xCl_2 \cdot 2H_2O$. In such materials interest centers on the spin glass behavior, which can result from the combined effects of frustration and randomness, and on the unusual and rather varied T-x phase diagram structures which occur.

The materials $MnCl_2 \cdot 2H_2O$, $FeCl_2 \cdot 2H_2O$, and $CoCl_2 \cdot 2H_2O$, which are the components of three of the mixed magnets listed above, form an isostructural series.[12] Their crystallographic similarity and magnetic characteristics made the various binary mixtures attractive to study. With the recent development of a corresponding series of monohydrate materials, the opportunity presents itself for studying the mixed magnetic system $Co_{1-x}Mn_xCl_2 \cdot H_2O$, the subject of this paper.

One component, $MnCl_2 \cdot H_2O$, has been shown[13] to behave as a quasi-one-dimensional (quasi-1D) Heisenberg antiferromagnet, ordering antiferromagnetically at 2.16 ± 0.01 K (2.18 ± 0.01 K by heat capacity data[14]) due to weak interchain exchange. The intrachain exchange interaction is $J/k = -0.49_3$ K (in $\hat{H}_{ex} = -2J\Sigma_{i>j}\hat{\mathbf{S}}_i \cdot \hat{\mathbf{S}}_j$). This is very similar to the interaction along $MnCl_2MnCl_2Mn\cdots$ chemical chains in three-dimensional $MnCl_2 \cdot 2H_2O$.[15] The interchain exchange $|J'/k| = 0.015 \pm 0.004$ K, as deduced from J and T_c, and probably antiferromagnetic, is down by a factor of 30 from that in the dihydrate. Analysis of heat capacity data supports these conclusions from susceptibility measurements. The inference is strong that $MnCl_2MnCl_2Mn\cdots$ chemical chains retain their integrity in the monohydrate, but that interchain exchange couplings, via chlorine-chlorine contacts and some hydrogen bonding, are drastically disrupted.

The magnetic behavior of $CoCl_2 \cdot H_2O$ is even more unusual.[16] A pronounced maximum in the susceptibility ap-

pears at 16.2 K, about 10% lower than T_{max} in $CoCl_2 \cdot 2H_2O$; moreover, the maximum susceptibility is about 5 times larger than that of the dihydrate.[17] The Weiss θ, in $\chi_M = C/(T - \theta)$, is strongly positive, implying that predominantly ferromagnetic interactions occur.[18] Yet an antiferromagnetic transition is inferred at 14.0 ± 0.1 K; this is 3.2 K lower than the antiferromagnetic transition in $CoCl_2 \cdot 2H_2O$. Heat capacity data actually reveal two transitions, each signaled by a similar size λ anomaly, at 15.0 ± 0.05 K and at 13.9 ± 0.05 K.[18] As for $MnCl_2 \cdot H_2O$, a relatively small critical magnetic entropy suggests a lower-dimensional magnetic lattice in $CoCl_2 \cdot H_2O$. But the more remarkable features are the magnetization irreversibility appearing in the 7–8 K range and the time dependence of the thermoremanent magnetization. Analysis of this reentrant spin glass behavior has been presented,[19] and it appears that the strong irreversibility line in $CoCl_2 \cdot H_2O$ conforms to expectations for a short-range Ising spin glass. In contrast to $MnCl_2 \cdot 2H_2O$, in which the predominant interactions are all antiferromagnetic, $CoCl_2 \cdot 2H_2O$ exhibits comparable interactions of both signs: ferromagnetic along $CoCl_2CoCl_2Co\cdots$ chains and antiferromagnetic between them.[17,20,21] It is very probable that these chains also retain their integrity in $CoCl_2 \cdot H_2O$. Variations in how water molecules are lost from the dihydrate lattice to form the monohydrate can lead to variations in local coordination geometry and thereby introduce microscopic randomness. Together with frustration effects from comparable interactions of mixed sign, the ingredients for spin glass formation occur. Presumably the absence of nonequilibrium phenomena in $MnCl_2 \cdot H_2O$ is because frustration among the antiferromagnetic interactions is at most very small.

In this paper we examine the mixed system $Co_{1-x}Mn_xCl_2 \cdot H_2O$ over the entire composition range, employing static magnetization and susceptibility measurements as a function of temperature, field, and time. The T-x phase diagram and the dependence of spin glass behavior on composition are major points of interest. We find that the magnetic behavior varies systematically with concentration and that a quite novel though incomplete T-x phase diagram can be inferred. The irreversibility is maximized in the $x = 0.3–0.4$ range. A reentrant spin glass state still occurs for $x = 0.30$, whereas for $x = 0.40$ and 0.50 the spin glass transition is not reentrant.

II. EXPERIMENT

The preparation of $MnCl_2 \cdot H_2O$ and $CoCl_2 \cdot H_2O$ has been described previously.[13,16] The materials are obtained by evaporation of an aqueous solution of the salts $MnCl_2 \cdot 4H_2O$ and $CoCl_2 \cdot 6H_2O$ at the same temperature of ca. 100 °C; therefore, in preparing various mixtures, these materials were dissolved in water in the desired mole fraction quantities. Each solution was evaporated to dryness at 100 ± 2 °C over a period of from 48 to 72 h, with occasional grinding to prevent occlusions of water from developing. Fine-grained polycrystalline material was obtained, and care was taken to minimize exposure to atmospheric water vapor. Thermogravimetric analysis confirmed that the monohydrate form had been obtained. Elemental analysis for cobalt and manganese by atomic absorption spectrometry gave values agreeing with nominal compositions to within 0.017 mole fraction unit rms, comparable with the experimental uncertainty. In the following nominal compositions are used.

Additional evidence that homogeneous mixed monohydrate material was obtained is provided by x-ray diffraction. Powder diffraction data for $MnCl_2 \cdot H_2O$ and $CoCl_2 \cdot H_2O$ in the literature are very similar.[22,23] In each case the pattern is distinguishable from that of the dihydrate system. In general, $CoCl_2 \cdot H_2O$ peaks occur at slightly larger diffraction angles (smaller d values) than peaks for $MnCl_2 \cdot H_2O$. Mixed material x-ray patterns displayed peaks corresponding to most of those expected for either pure monohydrate system; moreover, there was a general shifting of peaks from lower to higher diffraction angles as the fraction of manganese component decreased. There were no indications that either pure component was present separately. Thus, at the level probed by x rays, the mixed magnetic material appears microscopically homogeneous; magnetic characteristics of the samples, to be described, are also consistent with this.

Magnetization and susceptibility measurements were made using a variable temperature vibrating sample magnetometer system. Except where otherwise indicated, susceptibility data presented in the following are field-cooled measurements, with corrections (rather small) applied for demagnetization and diamagnetism. Polycrystalline samples of approximately 100 mg size were quickly packed under dry conditions into nonmagnetic sample holders, weighed, and then screwed onto a nonmagnetic sample rod in immediate proximity to a calibrated carbon-glass resistance thermometer. Temperatures are estimated to be accurate to ± 0.005–0.5 K, depending on the range, magnetic field values to $\pm \max(2\text{ G}, 0.1\%)$, and magnetization and susceptibility data to 1.5% absolute, with a precision much better than this. For zero-field-cooling experiments, a small external power supply was used to cancel the residual field of the 12″ electromagnet.

III. MEASUREMENTS AND ANALYSIS

A. Magnetic susceptibility

Inverse molar susceptibilities as a function of temperature for a series of polycrystalline samples of $Co_{1-x}Mn_xCl_2 \cdot H_2O$ are shown in Fig. 1. The data sets are fairly linear throughout most of the displayed temperature range, but some small degree of curvature is often present at higher T, especially for more cobalt rich mixtures. This is expected based on the previously analyzed behavior of $CoCl_2 \cdot H_2O$.[18] At temperatures near and below 20 K, obvious departures from linearity occur. A common fitting range of 29–70 K, where all data sets are quite linear, was chosen in order to obtain C and θ in the Curie-Weiss form $\chi_M = C/(T - \theta)$; this was also the range used in our earlier work on $CoCl_2 \cdot H_2O$.[18] The resulting Curie-Weiss constants, along with those of the pure components, appear in Fig. 2. Statistical uncertainties in these parameters are approximately ± 0.025 (emu K)/mol in C and ± 0.3 K in θ, which are comparable with the symbol sizes. Both C and θ vary with composition in a fairly smooth fashion; for θ, especially, the dependence on x is not simply linear. It is interesting that between $x = 0.8$ and 1 there is rather little variation in θ.

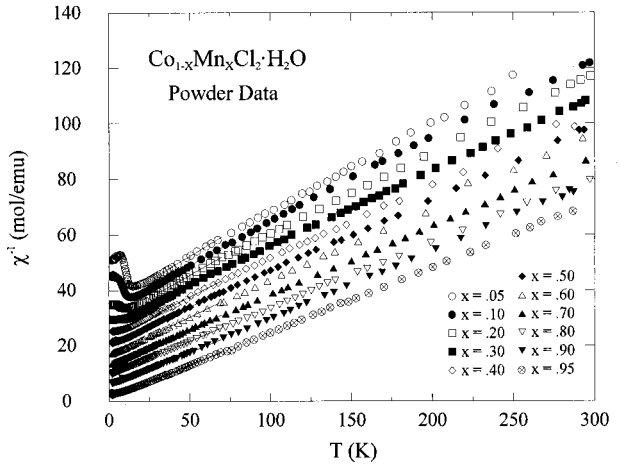

FIG. 1. Inverse molar magnetic susceptibility vs temperature for different compositions of $Co_{1-x}Mn_xCl_2 \cdot H_2O$. The $x=0.95$ set is unshifted, while reciprocal χ values for successively lower-x mixtures are shifted up by 4, 8, 12, etc. mol/emu, respectively. Lines correspond to Curie-Weiss fits in the 29–70 K range.

The molar susceptibility in the low-temperature region for various mixtures is shown in Figs. 3 and 4; measuring fields of approximately 100 or 200 G were used. In Fig. 3 it is evident that the location of a susceptibility maximum, which was found at 16.2 K in $CoCl_2 \cdot H_2O$, shifts to lower temperatures as the manganese content increases. The shape of the maximum also changes with composition. For the mixtures shown in Fig. 4, the susceptibilities are rather different in appearance from those in Fig. 3. A maximum still occurs for $x=0.40$, however. For $x=0.50$ the onset of a maximum is discernible at our lowest attainable temperature, but is not fully resolved. For $x=0.60$ no sign of a maximum is present. For these mixtures the susceptibilities also attain larger values than those in Fig. 3. For $x=0.80$ there is again no sign of a maximum; the minor feature near 2.2 K is instrumental. An $x=0.70$ data set, not shown, is similar to, with susceptibility values intermediate between, the $x=0.60$ and 0.80 sets. For $x=0.95$ and 0.90, susceptibility maxima are again present and located at successively lower temperatures than the 3.60 K maximum of $MnCl_2 \cdot H_2O$. The shapes of the two curves are different, the maximum being much broader for x

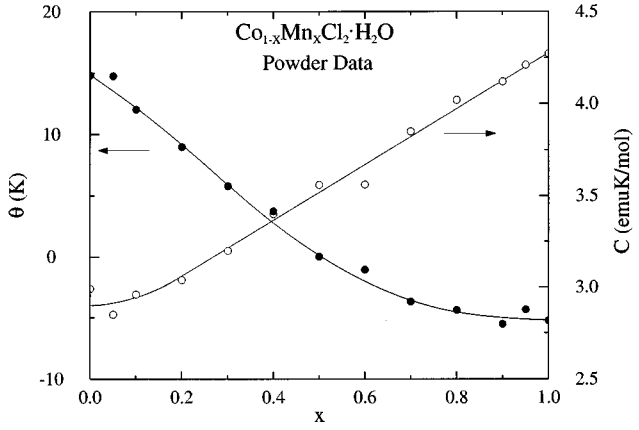

FIG. 2. Curie constant and Weiss θ vs composition for $Co_{1-x}Mn_xCl_2 \cdot H_2O$. Curves through results are guides to the eye.

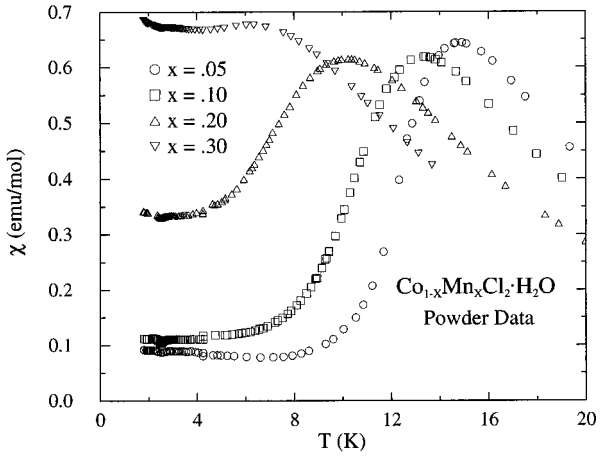

FIG. 3. Molar magnetic susceptibility vs temperature for various compositions of $Co_{1-x}Mn_xCl_2 \cdot H_2O$ rich in cobalt.

$=0.95$ and also displaying a double hump structure with maxima at 3.00 and 2.25 K. The $x=0.90$ data display an obvious maximum at 1.86 K and an incipient maximum, or shoulder, at 2.25 K.

From the data in Figs. 3 and 4, an estimate of T_{max}, the location of any susceptibility maximum present, was made. This quantity is displayed vs composition in Fig. 5; uncertainties are estimated to be ± 0.1–0.2 K, comparable with symbol size, except for $x=0.95$, where the uncertainty is about twice the symbol size. For $x=0.95$ and 0.90, the mean locations of the two maxima observed are plotted, 2.62 and 2.06 K, respectively.

Antiferromagnetic transition temperatures have also been estimated where possible. Such T_c are taken as the location of a maximum in $d\chi/dT$ on the low-temperature side of each peak if such an inflection point is discernible. Although theory identifies a maximum in $d(\chi T)/dT$ with an antiferromagnetic transition,[24] identifying $d\chi/dT$ is simpler and often employed. It was confirmed for various data sets here that the same T_c emerges using either approach. Thus, for $x=0.05$, 0.10, and 0.20, we estimate $T_c = 12.7_5$, 10.8_5, and 7.8_0 K, respectively; absolute uncertainties are ± 0.1–0.2 K.

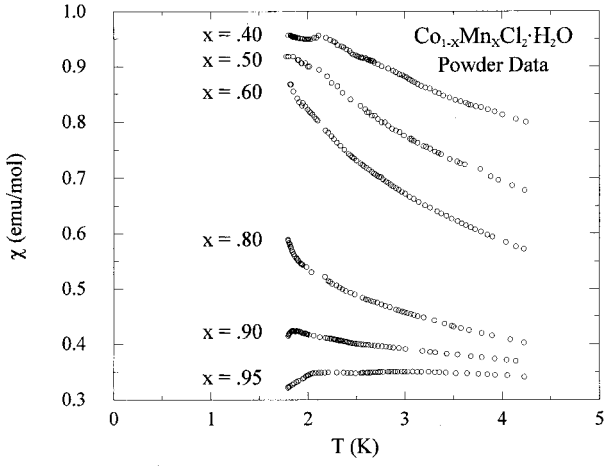

FIG. 4. Molar magnetic susceptibility vs temperature for remaining compositions of $Co_{1-x}Mn_xCl_2 \cdot H_2O$. For clarity, the $x=0.40$ data are shifted up 0.05 emu/mol.

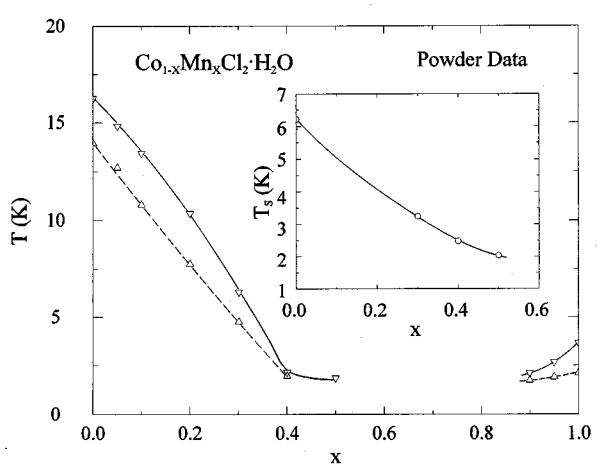

FIG. 5. Temperatures of susceptibility maxima (▽) and antiferromagnetic transitions (△) vs composition for $Co_{1-x}Mn_xCl_2 \cdot H_2O$. Curves through results are guides to the eye. The inset shows the strong irreversibility temperature, in a 0.2 kG measuring field, vs composition; see later text.

Such an inflection is not clearly evident for $x=0.30$ and 0.40; for these, T_c has been taken, somewhat arbitrarily, where a leveling in the susceptibility begins, at 4.8_0 and 2.0_3 K, respectively. For $x=0.50-0.80$, no T_c can be estimated. For $x=0.50$ a transition probably occurs several 0.1 K below the incipient maximum at 1.81 K. The absence of structure in the $x=0.60$, 0.70, and 0.80 susceptibilities suggests that any transition in these mixtures occurs well below 1.8 K. For $x=0.90$ and 0.95, close examination of the data reveals a marked drop in susceptibility, at 1.8_0 and 1.9_6 K, respectively, which we take to signify a transition. In Fig. 5 also appear the transition temperatures thus obtained; uncertainties are less than or comparable with symbol size.

B. Magnetization

For several mixtures magnetization vs field isotherms were measured at a series of temperatures from approximately 1.85 to 4.2 K and higher for $x=0.30$. The applied field was varied from 10 G to the maximum attainable 15.9 kG, then decreased back down. For cobalt-rich mixtures the isotherms are qualitatively similar to those of $CoCl_2 \cdot H_2O$,[19] displaying an inflection point in a generally increasing magnetization. There are, however, significant differences also. Several magnetization isotherms for $x=0.30$ appear in Fig. 6. Even for the lowest temperature of 1.863 K, the variation in curvature around the inflection point near 4 kG, the location of which shows no definite dependence on temperature up to at least 4.2 K, is much more gradual than for the pure cobalt material. The inflection also occurs at a somewhat lower field than the approximately 5 kG in $CoCl_2 \cdot H_2O$. A 4.24 K isotherm taken for the $x=0.20$ mixture also displayed an inflection near 4 kG; the variation in curvature was somewhat stronger than for the $x=0.30$ isotherms, but much weaker than for $CoCl_2 \cdot H_2O$ isotherms at a comparable temperature.[19] In Fig. 7 is shown the hysteresis of the lowest-temperature isotherm for $x=0.30$. The hysteresis is significant, but much smaller than for isotherms at comparable temperature or even as high as 5.974 K in $CoCl_2 \cdot H_2O$. It is

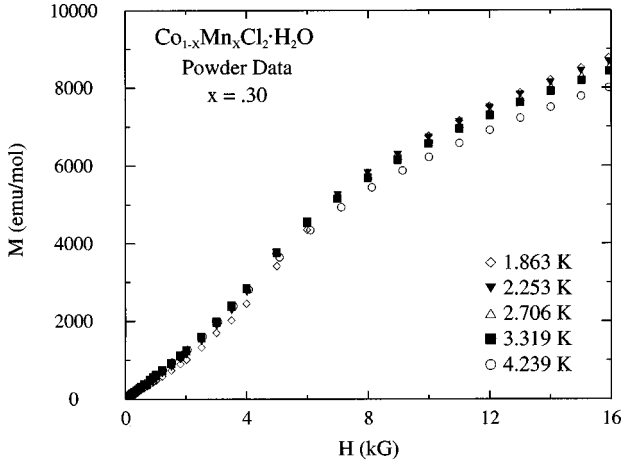

FIG. 6. Molar magnetization vs field (increasing) at various temperatures for an $x=0.30$ composition of $Co_{1-x}Mn_xCl_2 \cdot H_2O$.

comparable with the hysteresis of an 8.057 K isotherm in $CoCl_2 \cdot H_2O$, though the latter still displays a much greater variation in curvature. With increasing temperature the hysteresis displayed by the $x=0.30$ isotherms becomes progressively weaker and is barely discernible for 3.319 and 4.239 K. For $CoCl_2 \cdot H_2O$ it was not until temperatures of 12 K or greater were reached that the hysteresis became comparably small. Not until 13.94 K in the pure cobalt system did the curvature variation about the inflection point become comparable to that displayed by the isotherms of Fig. 6.

For $x=0.30$ isotherms were also taken at higher temperatures than those shown in Fig. 6. An inflection point in $M(H)$, still located near 4 kG, was discernible at 4.992 and 6.008 K, just barely so at 6.887 K, and was absent at 8.967 K. Hysteresis is essentially absent at 8.967 K. At yet larger temperatures, to as high as 20.19 K, there is only a gradual trend toward more nearly linear M vs H and toward smaller values of M generally. In $CoCl_2 \cdot H_2O$ there is an inflection point in $M(H)$ still detectable at 16.52 K; only at higher temperatures do $M(H)$ of uniform curvature emerge.

In Fig. 8 appear magnetization isotherms for $x=0.40$. Very interestingly, there is an evolution in the shape of $M(H)$ over the temperature range displayed. The 1.850 K

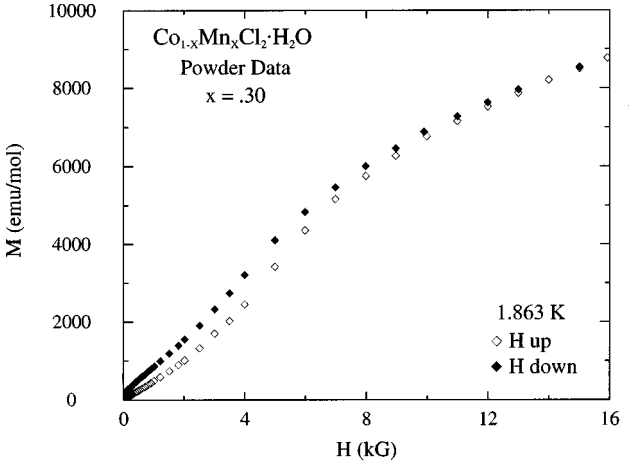

FIG. 7. Hysteresis in molar magnetization vs field at 1.863 K for an $x=0.30$ composition of $Co_{1-x}Mn_xCl_2 \cdot H_2O$.

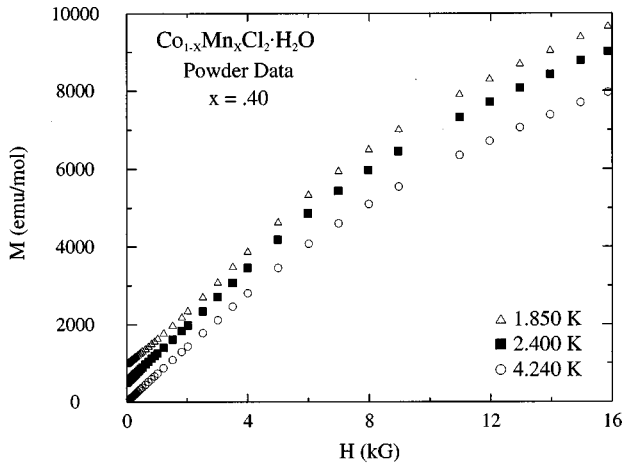

FIG. 8. Molar magnetization vs field (increasing) at various temperatures for an $x=0.40$ composition of $Co_{1-x}Mn_xCl_2\cdot H_2O$. For clarity, the 2.400 and 1.850 K isotherms are shifted up 500 and 1000 emu/mol, respectively.

isotherm exhibits an inflection point at 4 kG, though the variation in curvature is definitely weaker than in the 1.863 K isotherm of $x=0.30$ in Fig. 7. And while there is some hysteresis (not shown) in this 1.850 K isotherm, it is several times smaller than for $x=0.30$. The 2.400 K isotherm is not of the same shape. The variation in curvature is subtle and difficult to see in Fig. 8, but up to about 1.5 kG, $M(H)$ is concave downward; i.e., the second derivative is negative. Between 1.5 and 4 kG the curvature is very weakly concave upward; i.e., the second derivative is positive. Above 4 kG the curvature is again concave downward. Thus two inflection points occur, at 1.5 and 4 kG; the hysteresis is very small. The 4.240 K isotherm is yet different in shape. There are no inflection points, and the curvature is uniformly concave downward. The hysteresis is negligible.

In Fig. 9 appear magnetization isotherms for $x=0.50$. From 1.867 to 4.230 K all are of uniform curvature, without inflection points. The hysteresis (not shown) at 1.867 K is distinctly smaller than that of the 1.850 K isotherm of $x=0.40$; at higher temperatures, the hysteresis is negligible. The behavior in this mixture is therefore qualitatively different from that in $x=0.30$ and 0.40. It is significant that even the 1.867 K isotherm in Fig. 9 is at a temperature above that of the susceptibility maximum at 1.81 K. Yet in $x=0.40$, with $T_{max}=2.11$ K, the 2.400 K isotherm exhibited inflection points, while in $x=0.30$ inflections were discernible for $T \geqslant T_{max}$.

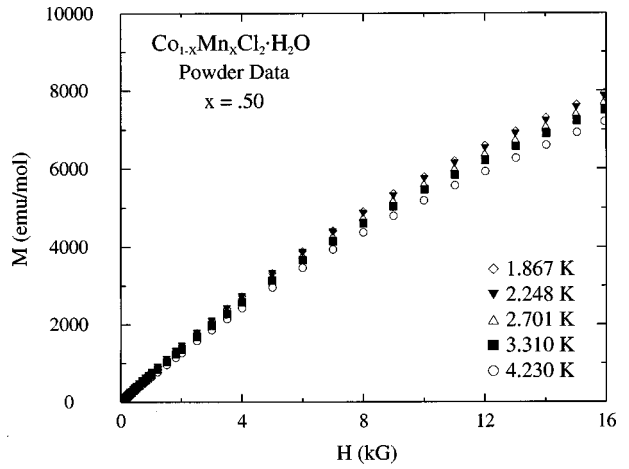

FIG. 9. Molar magnetization vs field (increasing) at various temperatures for an $x=0.50$ composition of $Co_{1-x}Mn_xCl_2\cdot H_2O$.

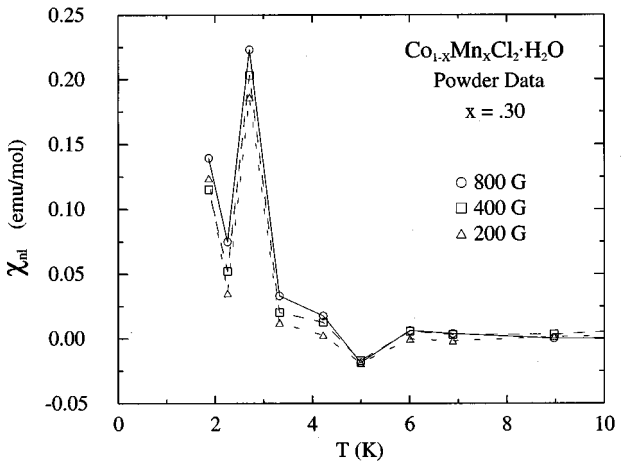

FIG. 10. Nonlinear susceptibility vs temperature at selected fields for an $x=0.30$ composition of $Co_{1-x}Mn_xCl_2\cdot H_2O$.

Magnetization isotherms were also obtained for several mixtures richer in the manganese component. At ca. 1.85 K these displayed uniform curvature similar to that of $x=0.50$ in Fig. 9, without inflections and with a greater tendency toward linear behavior as x increased. The hysteresis was negligible for x higher than 0.60. Isotherms at 4.2 K were without hysteresis altogether and also became increasingly linear as x increased. At either of these temperatures, the maximum magnetization, attained at 15.9 kG, decreased with increasing x.

C. Nonlinear susceptibility

For the $x=0.30$ mixture, each isotherm was analyzed to extract the nonlinear susceptibility,

$$\chi_{nl}(H,T)=\chi_0(T)-M(H,T)/H, \tag{1}$$

where $\chi_0=\lim_{H\to 0}(M/H)$ is obtained from the low-field portion of each magnetization curve. That is, the magnetization is taken to be expressible as a power series in H, sometimes written in the form

$$M=\chi_0 H-b_3(T)(\chi_0 H)^3+b_5(T)(\chi_0 H)^5-\cdots=(\chi_0-\chi_{nl})H. \tag{2}$$

In Fig. 10 appears $\chi_{nl}(H,T)$ deduced in this way based on field-cooled magnetization isotherms.

The nonlinear susceptibility in Fig. 10 is generally several times smaller than that obtained in the same way for $CoCl_2\cdot H_2O$.[19] From 9 to 6 K, χ_{nl} is nearly zero and exhibits negligible variation. An obvious minimum, with negative values, occurs at 4.99 K. From here to 3.32 K, a gradual increase occurs, followed by a sharp rise to a pronounced maximum at 2.71 K, and then another strong increase between 2.25 and 1.86 K. The appearance is in some respects

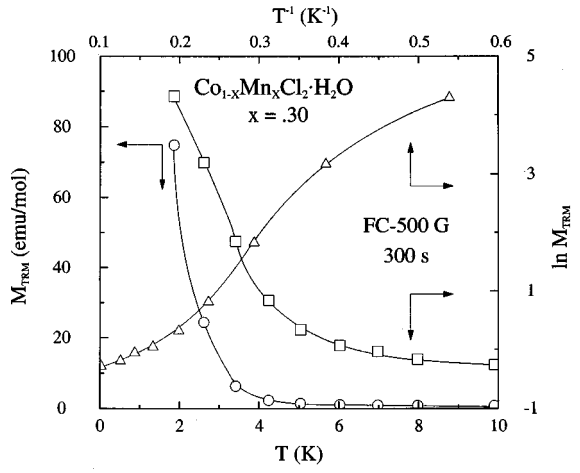

FIG. 11. Thermoremanent magnetization vs temperature for an $x=0.30$ composition of $Co_{1-x}Mn_xCl_2\cdot H_2O$, after 500 G field cooling and measured at 300 s. Arrows indicate axes for alternative representations; curves through data are guides to the eye.

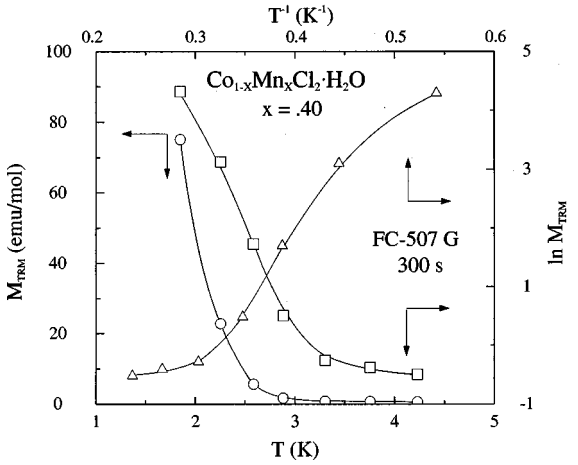

FIG. 12. Thermoremanent magnetization vs temperature for an $x=0.40$ composition of $Co_{1-x}Mn_xCl_2\cdot H_2O$, after 507 G field cooling and measured at 300 s. Arrows indicate axes for alternative representations; curves through data are guides to the eye.

similar to that for $CoCl_2\cdot H_2O$, and as there, the observed peak does not seem strong enough to be described as a divergence.

D. Thermoremanent magnetization

The thermoremanent magnetization (TRM) was examined for the $x=0.30$, 0.40, and 0.50 mixtures. It is measured by cooling the sample in an applied field from an initial temperature above any spin glass transition T_g to some final temperature, decreasing the field to zero and observing the decaying remanent magnetization. TRM data were taken after cooling in fields of either 0.5 or 5 kG, as in the earlier work on $CoCl_2\cdot H_2O$.[19] The initial temperature was above 20 K.

1. Temperature dependence

The temperature dependence of the TRM in the $x=0.30$ mixture, from observations made 300 s after turning off a 500 G cooling field, appears in Fig. 11. The $M_{\rm TRM}$ vs T representation shows a marked upturn below about 3.4 K. In order to check for the possibility of an activation process for the growth of the TRM, $M_{\rm TRM}\propto\exp(T^*/T)$, with T^* a characteristic temperature (energy), a $\ln M_{\rm TRM}$ vs $1/T$ plot was constructed. From the lack of linearity of this representation in Fig. 11, such a form is inadequate. Nor is linearity apparent in the $\ln M_{\rm TRM}$ vs T representation shown, which rules out a form like $M_{\rm TRM}\propto\exp(-\beta T)$, as has sometimes been reported for spin glasses. Not shown in Fig. 11 is a plot of $\ln M_{\rm TRM}$ vs $\ln T$, which is also nonlinear, thus eliminating the form $M_{\rm TRM}\propto T^{-c}$. In each of the last three representations, an inflection point occurs near the 3.41 K datum.

Similar plots for $x=0.40$ and 0.50 appear in Figs. 12 and 13. The appearance of the representations is rather similar to those of $x=0.30$, and none show linearity. For $x=0.40$, inflection points can be located in each representation other than the direct $M_{\rm TRM}$ vs T in the vicinity of the 2.58 K datum. For $x=0.50$, inflection points occur in the region spanned by the 2.05 and 2.14 K data. The corresponding representations of the TRM in $CoCl_2\cdot H_2O$, measured under similar conditions, appeared rather different, and no inflection points were present.[19] However, in the $\ln M_{\rm TRM}$ vs T representation appeared a clear crossover near 6 K between two linear regimes.

2. Cooling field dependence

The appearance of the various TRM(T) representations for $x=0.40$ and 0.50 after 5 kG cooling was similar to the corresponding plots after 0.5 kG cooling. Inflection points occurred in essentially the same temperature regions. The enhancement of the TRM at 1.85 K by the tenfold field enhancement was rather modest, by about 55% for $x=0.40$ and about 32% for $x=0.50$ near $t=0$. This is very much in contrast to the behavior in $CoCl_2\cdot H_2O$, where (a) corresponding TRM(T) representations had quite different appearance after 5 kG vs 0.5 kG field cooling and (b) the TRM was approximately two orders of magnitude larger at 1.9 K after 5 kG

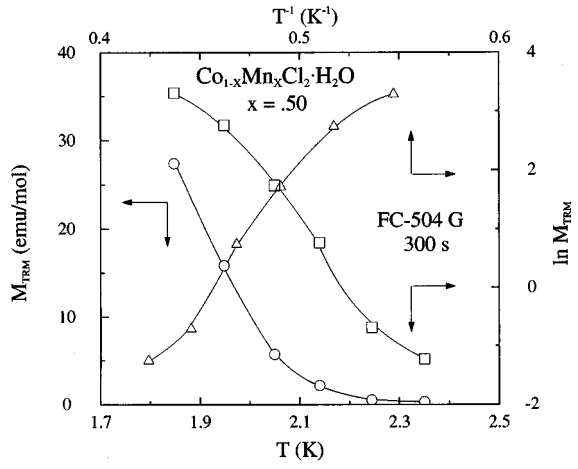

FIG. 13. Thermoremanent magnetization vs temperature for an $x=0.50$ composition of $Co_{1-x}Mn_xCl_2\cdot H_2O$, after 504 G field cooling and measured at 300 s. Arrows indicate axes for alternative representations; curves through data are guides to the eye.

than after 0.5 kG cooling. For $x=0.30$, differences in the appearance of TRM(T) representations for 5 and 0.5 kG field cooling occurred, but these were less pronounced than for $CoCl_2\cdot H_2O$. The TRM at 1.8 K near $t=0$ was about 2.5 times larger after 5 kG than after 0.5 kG cooling. This is a much stronger field effect than for the $x=0.40$ and 0.50 mixtures, but is still much less than for $CoCl_2\cdot H_2O$. An observation can be made that applies to both $CoCl_2\cdot H_2O$ and the mixtures: the TRM (at fixed measuring time) falls more rapidly with increasing temperature for the larger 5 kG field than for 0.5 kG.

3. Composition dependence

From the above and the results on $CoCl_2\cdot H_2O$ previously,[19] several observations concerning the composition dependence of the TRM can be made. It is evident from Figs. 11–13 that the 0.5 kG TRM decreases more rapidly with increasing T as x increases. Thus in $CoCl_2\cdot H_2O$ the ratio of the TRM (measured 300 s after turning off a 507 G cooling field) at 4.227 and 6.989 K to the TRM at 1.899 K is 0.57 and 0.20, respectively. Using comparable data as a reference (at ~1.85 K in each case), for $x=0.30$, the TRM at 2.61 and 3.41 K is only 0.33 and 0.085 as large, respectively; for $x=0.40$, the TRM at 2.25 and 2.58 K is only 0.30 and 0.075 as large, respectively; and for $x=0.50$, the TRM at 2.05 and 2.14 K is only 0.21 and 0.078 as large, respectively.

Employing for each sample very similar temperatures to those of the 0.5 kG TRM surveyed just above, one obtains corresponding ratios for 5 kG field cooling: $x=0$, 0.125, and 0.0075; $x=0.30$, 0.15, and 0.028; $x=0.40$, 0.20, and 0.050; and $x=0.50$, 0.19, and 0.078. The trend is still evident for 5 kG, but is less pronounced. Also apparent, if imperfectly, is that (as already noted) the TRM falls faster with increasing temperature for 5 kG than for 0.5 kG field cooling.

As previously observed, the TRM increases less rapidly with cooling field as x increases. The results of the next section will show that the TRM, for a given temperature and cooling field, also decreases faster with time as x increases. Some observations on the magnitude of the TRM near 1.85 K can also be made. For 0.5 kG field cooling, the TRM is almost an order of magnitude larger for $x=0.30$ than for $x=0$, it is virtually unchanged from $x=0.30$ to 0.40, and it is smaller by a factor of nearly 3 in $x=0.50$ than in $x=0.40$. For 5 kG field cooling, however, the TRM near 1.85 K is 5–6 times smaller for $x=0.30$ than for $x=0$; it is smaller by a factor of 2 in $x=0.40$ and by a factor of 6 in $x=0.50$ than in $x=0.30$.

4. Time dependence

For each of the mixtures $x=0.30$, 0.40, and 0.50, the time dependence of the TRM, for various temperatures and cooling fields, was followed for 2400 s, except where experimental constraints led to shorter periods. In order to test for possible algebraic ($M_{\mathrm{TRM}}\propto t^{-a}$) or logarithmic time dependences, plots of $\log_{10} M_{\mathrm{TRM}}$ vs $\log_{10} t$ and of M_{TRM} vs $\log_{10} t$ were constructed. These were not generally linear, and so the decay does not follow either of these simple forms.

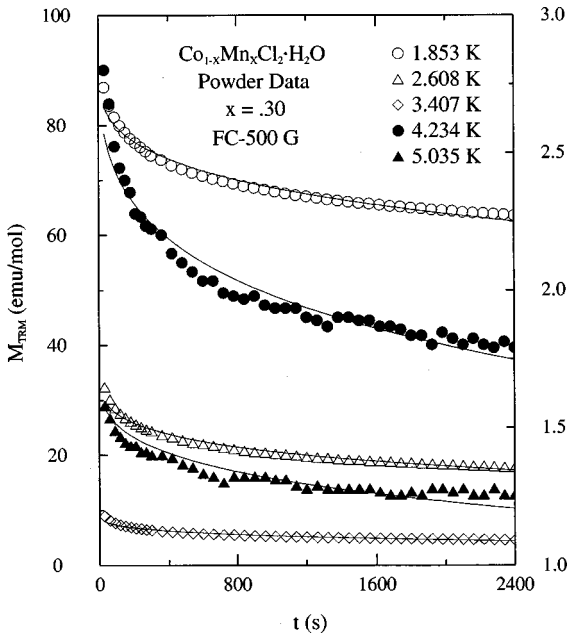

FIG. 14. Time dependence of thermoremanent magnetization at different temperatures after 500 G field cooling of an $x=0.30$ composition of $Co_{1-x}Mn_xCl_2\cdot H_2O$. Solid symbols are referred to the right-hand scale. Curves are stretched exponential fits, Eq. (3), described in the text.

Each $M_{\mathrm{TRM}}(t)$ set was fit using a stretched exponential form

$$M_{\mathrm{TRM}}(t)=M_0\exp[-(t/\tau)^b]. \tag{3}$$

This expression has often been shown to provide a plausible, if imperfect, approximation where simpler dependences do not occur. Initial fitting attempts in which b varied along with M_0 and τ sometimes gave slightly better fits than those to be presented. But the resulting b varied erratically, while the M_0 and τ values differed little from those to be shown. Therefore, as in our earlier work on $CoCl_2\cdot H_2O$, a fixed b was adopted; a survey of plausible values suggested $b=0.33$ as best.

In Figs. 14–19 are shown the TRM fits according to Eq. (3) for the $x=0.30$, 0.40, and 0.50 mixtures and both cooling fields. The quality of the fits is variable, rms deviations ranging from 1.2% to 4.6% in most cases. Substantial efforts at improving the lesser quality fits were unsuccessful.

The dependence of the parameters M_0 and τ on temperature appears in Figs. 20–22. The prefactor M_0 for $x=0.30$, Fig. 20, decreases monotonically with increasing temperature for each cooling field. For each, the approach to vanishing M_0 becomes more gradual with increasing T, behavior which contrasts with the nearly linear variation in T occurring for $CoCl_2\cdot H_2O$,[19] especially for 0.5 kG cooling. Hence extrapolations to $M_0=0$ are somewhat uncertain, though the results suggest that this occurs at a higher temperature (5.5–6 K) for 0.5 kG than for 5 kG (4.5–5 K). The temperature dependence of τ is also qualitatively different from that for $CoCl_2\cdot H_2O$, in particular for 0.5 kG cooling. Near 1.8 K the fitted τ value, ca. 4.65×10^4 s, is nearly two orders of magnitude smaller than in $CoCl_2\cdot H_2O$ for similar temperature and cooling field. As in the pure material, there is an

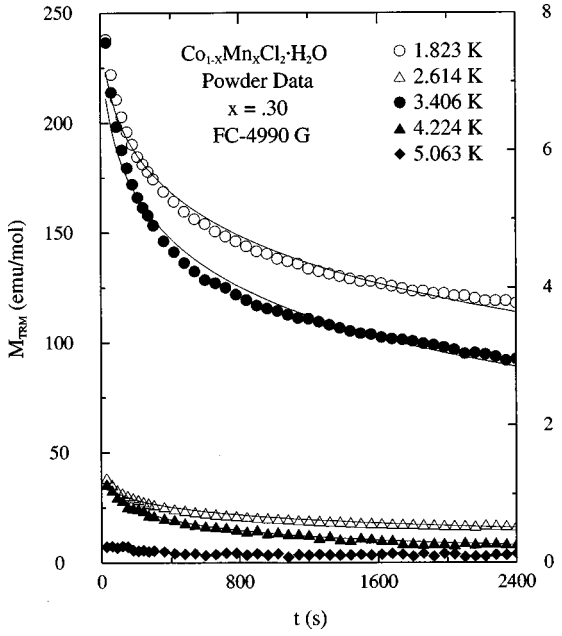

FIG. 15. Time dependence of thermoremanent magnetization at different temperatures after 4990 G field cooling of an $x=0.30$ composition of $Co_{1-x}Mn_xCl_2\cdot H_2O$. Solid symbols are referred to the right-hand scale. Curves are stretched exponential fits, Eq. (3), described in the text.

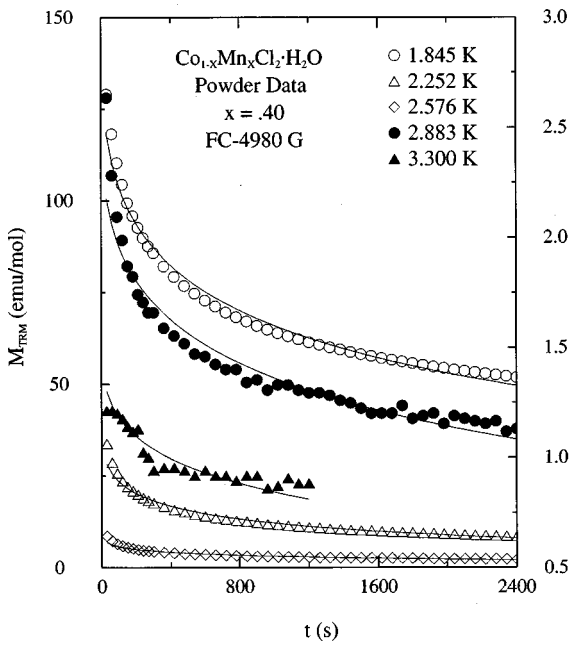

FIG. 17. Time dependence of thermoremanent magnetization at different temperatures after 4980 G field cooling of an $x=0.40$ composition of $Co_{1-x}Mn_xCl_2\cdot H_2O$. Solid symbols are referred to the right-hand scale. Curves are stretched exponential fits, Eq. (3), described in the text.

initial decrease in τ with increasing T. But in the mixture this weakens markedly between 2.6 and 3.4 K, and an increasing τ with increasing T sets in above 3.4 K. For the 5 kG cooling field data τ values are several times smaller, typically, than for 0.5 kG, and a decreasing τ with increasing T persists through 4.2 K. Despite many attempts, a fit to the 5.063 K TRM data, shown in Fig. 15, was not obtained. However, it is evident from the almost negligible time dependence of this set that a rather large time constant must obtain. Therefore an upturn in τ from 4.2 to 5 K in Fig. 20 can be assumed. The upturn occurs at a higher temperature for the 5 kG than for the 0.5 kG $\tau(T)$.

The M_0 and τ dependences for $x=0.40$ in Fig. 21 are qualitatively similar to those described for $x=0.30$. In gen-

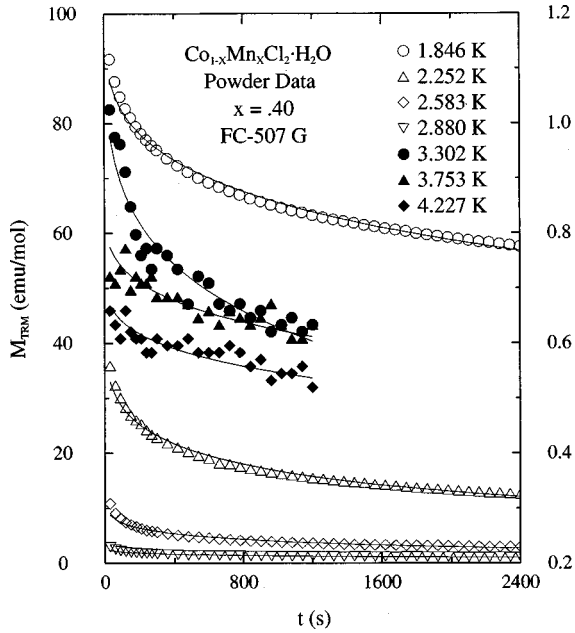

FIG. 16. Time dependence of thermoremanent magnetization at different temperatures after 507 G field cooling of an $x=0.40$ composition of $Co_{1-x}Mn_xCl_2\cdot H_2O$. Solid symbols are referred to the right-hand scale. Curves are stretched exponential fits, Eq. (3), described in the text.

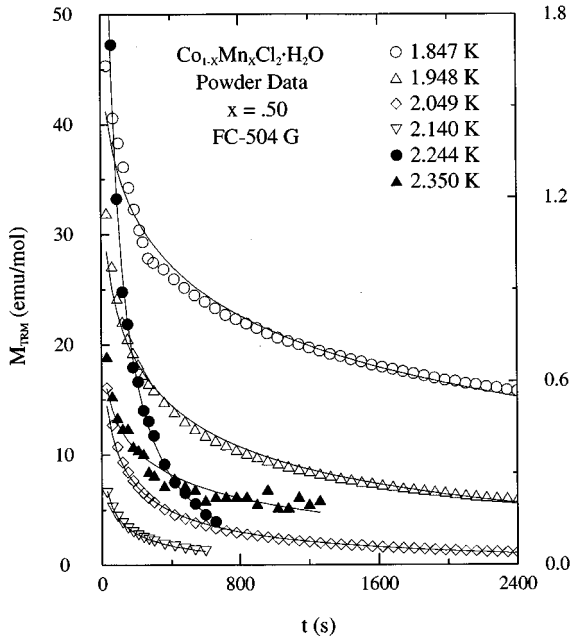

FIG. 18. Time dependence of thermoremanent magnetization at different temperatures after 504 G field cooling of an $x=0.50$ composition of $Co_{1-x}Mn_xCl_2\cdot H_2O$. Solid symbols are referred to the right-hand scale. Curves are stretched exponential fits, Eq. (3), described in the text.

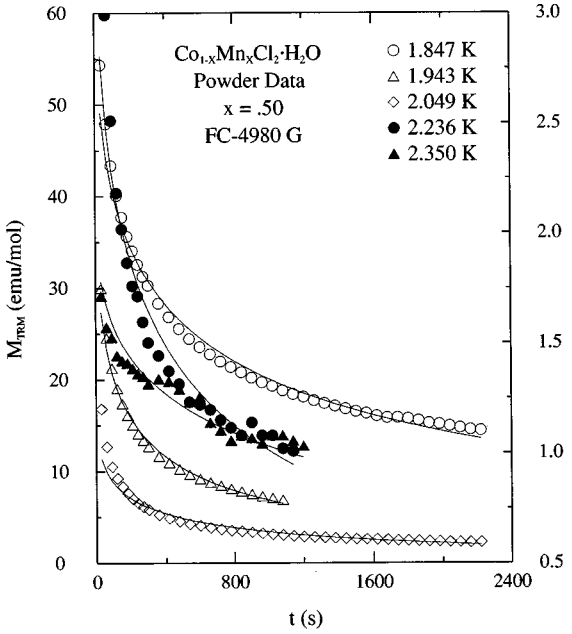

FIG. 19. Time dependence of thermoremanent magnetization at different temperatures after 4980 G field cooling of an $x=0.50$ composition of $Co_{1-x}Mn_xCl_2\cdot H_2O$. Solid symbols are referred to the right-hand scale. Curves are stretched exponential fits, Eq. (3), described in the text.

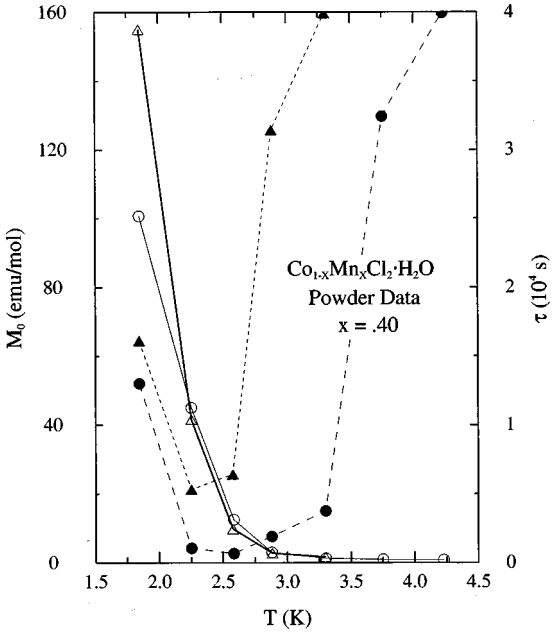

FIG. 21. Temperature dependence of prefactor M_0 and relaxation time τ in stretched exponential fits to thermoremanent magnetization decay in an $x=0.40$ composition of $Co_{1-x}Mn_xCl_2\cdot H_2O$. Circles are 507 G and triangles 4980 G field cooling results. Open symbols are M_0 referred to the left-hand scale, and solid symbols are τ referred to the right-hand scale; for solid triangles, the depicted values are 10 times larger than actual. Lines are guides to the eye only.

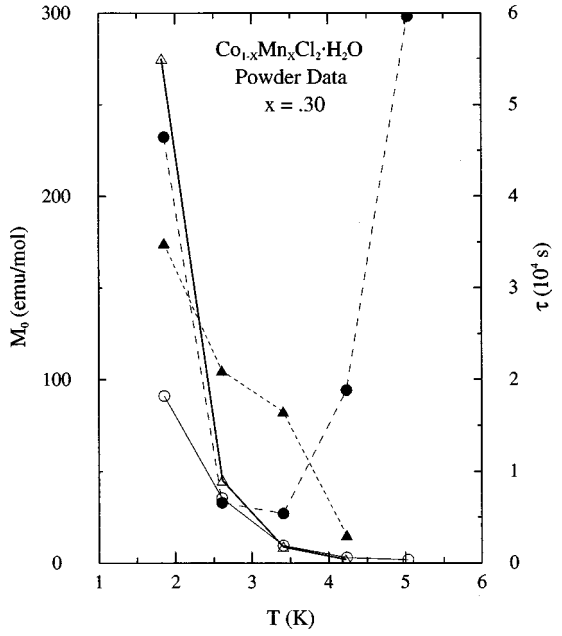

FIG. 20. Temperature dependence of prefactor M_0 and relaxation time τ in stretched exponential fits to thermoremanent decay in an $x=0.30$ composition of $Co_{1-x}Mn_xCl_2\cdot H_2O$. Circles are 500 G and triangles 4990 G field cooling results. Open symbols are M_0 referred to the left-hand scale, and solid symbols are τ referred to the right-hand scale; for solid triangles, the depicted values are 10 times larger than actual. Lines are guides to the eye only.

eral, both parameters are smaller, for similar temperature and cooling field, than those of $x=0.30$. As there, an extrapolation of $M_0(T)$ to vanishing M_0 is uncertain, but the results suggest that this again occurs at a higher temperature for 0.5 kG (4.5–5 K) than for 5 kG (3.5–4 K). These temperature estimates are lower than the corresponding ones for $x=0.30$. For both cooling fields, τ for $x=0.40$ first decreases with increasing T and then exhibits an upturn, which sets in between 2.6 and 2.9 K for 0.5 kG and between 2.2 and 2.6 K for 5 kG. In contrast to the situation for $x=0.30$, then, for $x=0.40$ the upturn occurs at a slightly higher temperature for 0.5 kG than for 5 kG. As for $x=0.30$, however, τ values tend to be somewhat smaller for the 5 kG field.

The M_0 and τ dependences for $x=0.50$ in Fig. 22 are, with one exception, similar to those just described. In general, both parameters are smaller, for similar temperature and cooling field, than those of $x=0.40$. Extrapolation of $M_0(T)$ for 5 kG cooling to vanishing M_0 is uncertain, but a plausible estimate is 2.5–3 K. The $M_0(T)$ for 0.5 kG is exceptional in that a nearly linear temperature dependence occurs and extrapolation to vanishing M_0 at 2.35 K can be made; moreover, this is below, rather than above, that just estimated for 5 kG. Both estimates are significantly lower than those obtained for $x=0.40$, and it is clear that $T'(M_0=0)$ decreases with increasing x. For both cooling fields, τ first decreases with increasing T and then turns up, between 2.24 and 2.35 K for 0.5 kG and between 1.94 and 2.05 K for 5 kG. The upturn occurs at a significantly higher temperature for the lower field, a much more pronounced manifestation of the tendency observed in $x=0.40$ and contrasting with that in $x=0.30$. For lower temperatures, τ values are somewhat smaller for 5 kG than for 0.5 kG, rather as for the $x=0.30$ and 0.40 mixtures.

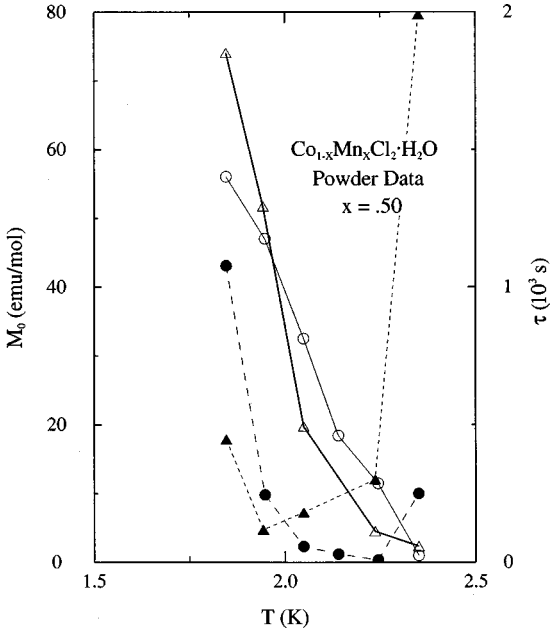

FIG. 22. Temperature dependence of prefactor M_0 and relaxation time τ in stretched exponential fits to thermoremanent magnetization decay in an $x=0.50$ composition of $Co_{1-x}Mn_xCl_2\cdot H_2O$. Circles are 504 G and triangles 4980 G field cooling results. Open symbols are M_0 referred to the left-hand scale, and solid symbols are τ referred to the right-hand scale. Lines are guides to the eye only.

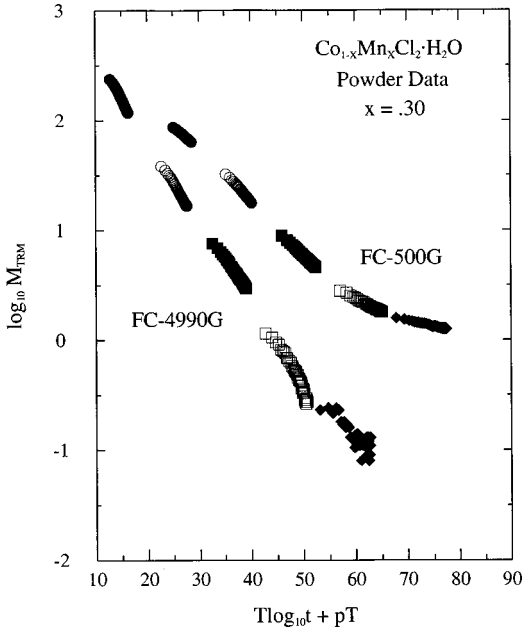

FIG. 23. Optimal $T\log_{10}(t/\tau_0)$ scaling plots for thermoremanent magnetization decay in an $x=0.30$ composition of $Co_{1-x}Mn_xCl_2\cdot H_2O$. For the 500 G data $p=12$ ($\tau_0=10^{-12}$ s) and for the 4990 G data $p=11$ ($\tau_0=10^{-11}$ s). For clarity, the 4990 G sets are shifted down 10 units along the horizontal axis.

5. $T\log_{10}(t/\tau_0)$ scaling

It has been proposed[25] that the TRM in spin glasses should scale as $T\log_{10}(t/\tau_0)$, where τ_0 is a microscopic spin flip time. This has been observed in CuMn,[25] in our previous work on $CoCl_2\cdot H_2O$,[19] and has also been obtained in simulations of both infinite- and short-range spin glass models.[26] It can, in fact, be expected whenever relaxation occurs by thermal activation over barriers for which the barrier height distribution is independent of temperature. Relaxation in small particle systems also scales in this way.[27,28]

In order to test the scaling form in $Co_{1-x}Mn_xCl_2\cdot H_2O$ plots of $\log_{10} M_{\rm TRM}$ vs $T\log_{10} t+pT$ were constructed for each of the TRM sets. Different p $(=-\log_{10}\tau_0)$ correspond to different τ_0, and examination of plots constructed for different p readily discloses an optimal τ_0 if such exists. In Figs. 23–25 appear the optimal scaling plots for $x=0.30$, 0.40, and 0.50 for the two cooling fields. Except for some higher-temperature TRM segments, satisfactory scaling is obtained. Rather similar τ_0 values emerge: 10^{-12} s for both cooling fields in $x=0.40$, 10^{-13} s for both cooling fields in $x=0.50$, and 10^{-11} and 10^{-12} s for the larger and smaller cooling fields in $x=0.30$. The precision of the p estimates is of order unity, and so the τ_0 are determined to within one order of magnitude.

E. Irreversibility lines

Zero-field-cooled and field-cooled magnetizations were measured for certain mixtures, using applied fields ranging from 25 G to 5 kG. The most detailed examination was performed on an $x=0.30$ mixture. Two examples appear in Fig. 26. Smooth curves were drawn through the data, and the difference between $M_{\rm FC}/H$ and $M_{\rm ZFC}/H$ obtained every 0.25 K. This difference, the irreversible magnetization $M_{\rm IRR}$ divided by H, is then plotted vs T. The results for the data of Fig. 26 are shown in Fig. 27. There appears a region at higher temperature where $M_{\rm IRR}/H$ is rather small and a region at lower temperature where it is much larger. One esti-

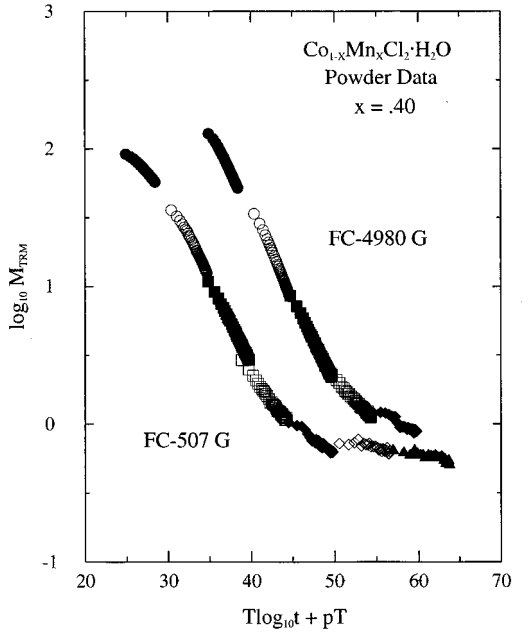

FIG. 24. Optimal $T\log_{10}(t/\tau_0)$ scaling plots for thermoremanent magnetization decay in an $x=0.40$ composition of $Co_{1-x}Mn_xCl_2\cdot H_2O$. For both cooling fields $p=12$ ($\tau_0=10^{-12}$ s). For clarity, the 4980 G sets are shifted up 10 units along the horizontal axis.

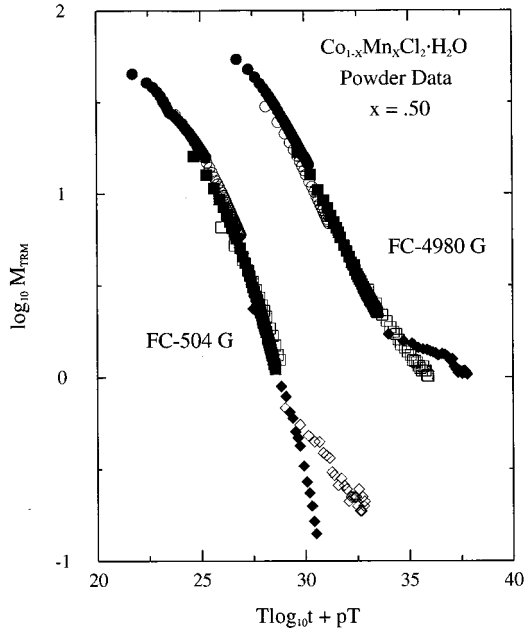

FIG. 25. Optimal $T\log_{10}(t/\tau_0)$ scaling plots for thermoremanent magnetization decay in an $x=0.50$ composition of $Co_{1-x}Mn_xCl_2 \cdot H_2O$. For both cooling fields $p=13$ ($\tau_0=10^{-13}$ s). For clarity, the 504 G sets are shifted down 5 units along the horizontal axis.

mates, as indicated in the figure, temperatures (T_w) where the weak irreversibility begins and temperatures (T_s) where the strong irreversibility begins based on linear approximations to M_{IRR}/H vs T in the two regions.[29]

In Fig. 28 is shown the strong irreversibility line for $x=0.30$, along with a fit using a recent prediction for the short-range 3D Ising spin glass[30] and (inset) an empirical power law fit. Spin glass irreversibility lines are predicted to take the form $\tau_g \propto h^a$, where the reduced temperature $\tau_g = [1-T_g(H)/T_g(0)]$, where the reduced field $h = \mu H/kT_g(0)$, with the spin magnetic moment μ equal to $g\mu_B[S(S+1)]^{1/2}$ and where a is a simple fraction or an integer.[31–33]

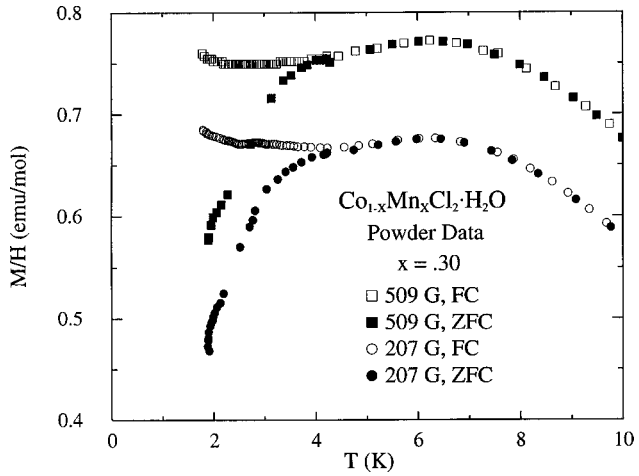

FIG. 26. Temperature dependence of field-cooled and zero-field-cooled magnetizations divided by field for two measuring fields in an $x=0.30$ composition of $Co_{1-x}Mn_xCl_2 \cdot H_2O$. For clarity, the 509 G data are shifted up 0.1 emu/mol.

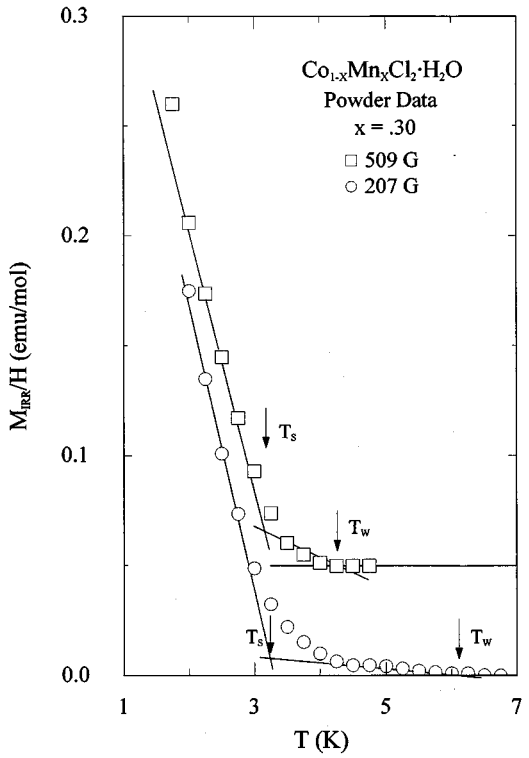

FIG. 27. Irreversible magnetization divided by field ($M_{\mathrm{FC}}/H - M_{\mathrm{ZFC}}/H$) vs temperature for two measuring fields in an $x=0.30$ composition of $Co_{1-x}Mn_xCl_2 \cdot H_2O$. For clarity, the 509 G results are shifted up 0.05 emu/mol. Estimated temperatures for the onset of strong irreversibility (T_S) and weak irreversibility (T_W) are indicated.

A review of the main results of mean-field theory in the best-studied model of infinite-range interactions, including the effects of anisotropy, appears in Ref. 19. The most common experimental situation, in various kinds of spin glasses,[29,34,35] is one in which first the transverse spin components of a predominantly Heisenberg spin glass freeze,

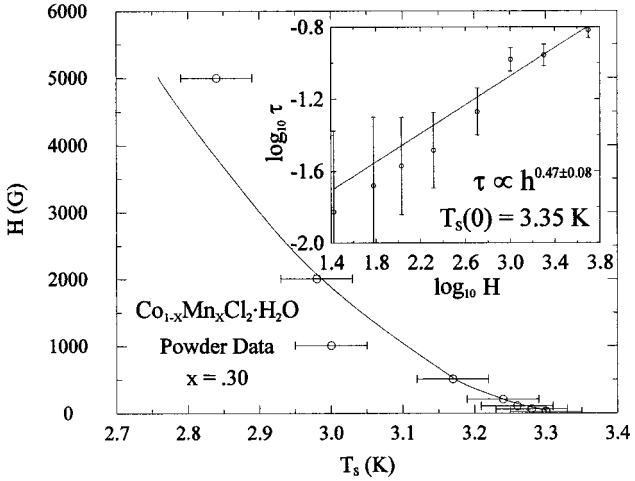

FIG. 28. Strong irreversibility line for an $x=0.30$ composition of $Co_{1-x}Mn_xCl_2 \cdot H_2O$. The curve shown is a fit based on a recent prediction for a short-range 3D Ising spin glass ($\tau_g \propto h^{0.53}$). The inset shows an unbiased determination of the optimal exponent a in $\tau_g \propto h^a$.

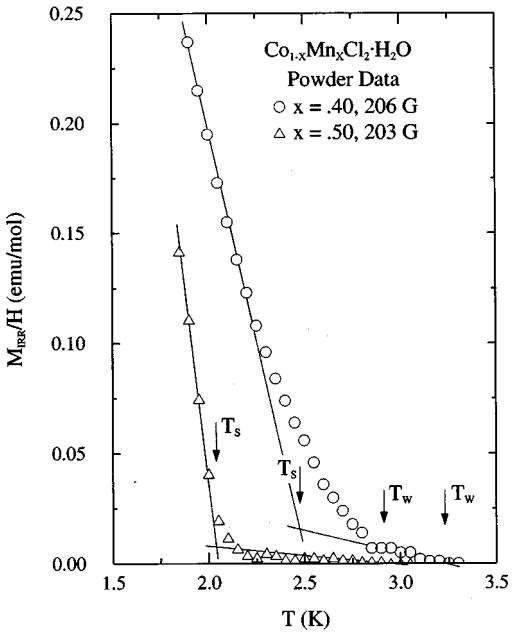

FIG. 29. Irreversible magnetization divided by field ($M_{FC}/H - M_{ZFC}/H$) vs temperature for $x=0.40$ and 0.50 compositions of $Co_{1-x}Mn_xCl_2\cdot H_2O$. Estimated temperatures for onset of strong irreversibility (T_S) and weak irreversibility (T_W) are indicated.

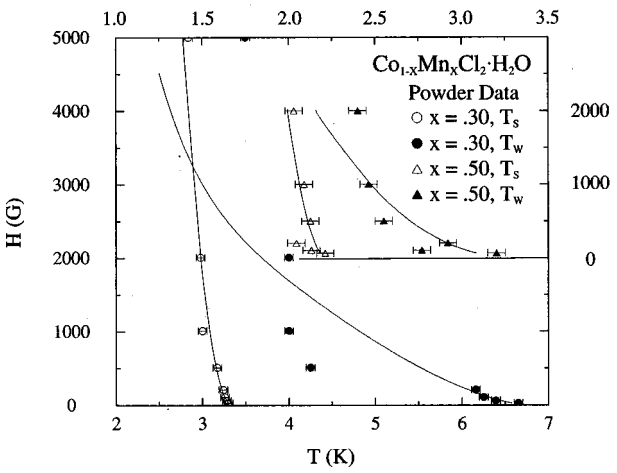

FIG. 30. Strong and weak irreversibility lines for $x=0.30$ and 0.50 compositions of $Co_{1-x}Mn_xCl_2\cdot H_2O$. The $x=0.50$ results are with respect to the upper-temperature scale and the right-field scale with zero level shifted up. Curves through results are fits described in the text according to a $\tau_g \propto h^a$ form.

along a Gabay-Toulouse-like line with $\tau_g \propto h^2$, followed by freezing of the longitudinal spin component, in a more strongly irreversible way, along a DeAlmeida-Thouless-like line with $\tau_g \propto h^{2/3}$. Our results for $Co_{1-x}Mn_xCl_2\cdot H_2O$ and those obtained previously for $CoCl_2\cdot H_2O$ differ from predictions of the infinite-range mean-field model.

The curve in the main part of Fig. 28 is according to Ritort's result,[30] $\tau_g \propto h^{0.53}$, for a short-range 3D Ising spin glass, with $T_s(0)=3.35$ K. This form gave a better fit to the strong irreversibility line in $CoCl_2\cdot H_2O$ than did the DeAlmeida-Thouless form $\tau_g \propto h^{2/3}$ and does so here also. The inset shows a best fit line via a double logarithmic representation; the exponent is 0.47 ± 0.08, quite similar to the value 0.53 and rather below the value 2/3.

Field-cooled and zero-field-cooled magnetizations were also collected on an $x=0.50$ mixture, using a somewhat narrower range of applied fields, and on an $x=0.40$ mixture using a 206 G field. In Fig. 29 are shown the M_{IRR}/H vs T results for $x=0.40$ and for an $x=0.50$ set using a similar applied field. The weak and strong irreversibility temperatures are noted. In Fig. 30 are shown the weak and strong irreversibility lines determined for $x=0.30$ and 0.50. The curves are in each case $\tau_g \propto h^a$ fits to $T_s(H)$ or $T_w(H)$. The specifics concerning $T_s(H)$ for $x=0.30$ have been given. For $T_s(H)$ of $x=0.50$, the parameters are $T_s(0)=2.22_7$ K and $a=0.49$. For $T_w(H)$, the parameters are $x=0.30$, $T_w(0)=6.75$ K, and $a=0.66$ and $x=0.50$, $T_w(0)=3.35$ K, and $a=0.43$. The exponents are not more precise than 0.08, and those for $x=0.50$ are somewhat less precise because the fits are less good. The close similarity of $T_s(0)$ for $x=0.30$ and $T_w(0)$ for $x=0.50$ is coincidental. The similarity of exponent values for the strong irreversibility lines of the two mixtures and their closer correspondence to the short-range 3D Ising model result than to the DeAlmeida-Thouless value of 2/3 are apparent. Possibly even more significant is that the exponents describing the weak irreversibility lines are both far below the Gabay-Toulouse value of 2.

For completeness and subsequent reference, the proportionality factors c, in $\tau_g = ch^a$, for each of the irreversibility lines are now given: $x=0.30$, $c=0.23_2$, and 2.0_8 for the strong and weak lines, respectively, and $x=0.50$, $c=0.17_9$, and 0.68_8 similarly. In obtaining these the value of μ in $h=\mu H/kT_g(0)$ was calculated from the observed Curie constants in Fig. 2 ($\mu=[3kC/N_0]^{1/2}$).

In Fig. 5 is shown the strong irreversibility temperature vs composition in $Co_{1-x}Mn_xCl_2\cdot H_2O$, using a 0.2 kG measuring field. The monotonic decrease of T_s is quite regular. Although the rate of variation decreases with increasing x, significantly lower temperatures than we can attain would be needed to study mixtures at higher x than 0.50.

IV. DISCUSSION

The T-x diagram of $Co_{1-x}Mn_xCl_2\cdot H_2O$, Fig. 5, is rather unusual. In mixed magnets with competing orthogonal anisotropies, $T_c(x)$ decreases from either composition extreme toward a tetracritical point. The ordered spin arrangements in the antiferromagnetic phases of $CoCl_2\cdot H_2O$ and $MnCl_2\cdot H_2O$ are not known, and so one cannot say if a tetracritical point is expected. In the corresponding dihydrate materials, orthogonal anisotropies are not present; nevertheless, $T_c(x)$ in $Co_{1-x}Mn_xCl_2\cdot 2H_2O$ does decrease from both ends of the phase diagram because of frustration that is induced on mixing. The rate of decrease of T_c with increasing x in $Co_{1-x}Mn_xCl_2\cdot H_2O$, i.e., $(\Delta T_c/T_c)/\Delta x$ in the $x=0-0.4$ interval, is approximately twice as large as in $Co_{1-x}Mn_xCl_2\cdot 2H_2O$. From $x=1$ to 0.90 the rate of decrease of T_c is just slightly greater in $Co_{1-x}Mn_xCl_2\cdot H_2O$, with $T_c(0.90)/T_c(1)=0.83$ and 0.87 in monohydrate and dihydrate mixtures. Also, in $Co_{1-x}Mn_xCl_2\cdot 2H_2O$, from $x=0$ to 0.5, $T_{max}(x)$, from susceptibility maxima, shows a definite concave downward curvature (dT_{max}/dx becomes more negative as x increases) and so does $T_c(x)$ in this region,

though more weakly so. In $Co_{1-x}Mn_xCl_2 \cdot H_2O$, $T_{max}(x)$, Fig. 5, has a clear concave downward curvature up to $x=0.4$, but $T_c(x)$ is concave upward (dT_c/dx becomes less negative as x increases). On the other side of the phase diagram, in $Co_{1-x}Mn_xCl_2 \cdot 2H_2O$ both $T_{max}(x)$ and $T_c(x)$ are weakly concave downward, at any rate from $x=1$ to 0.7. In $Co_{1-x}Mn_xCl_2 \cdot H_2O$, in the restricted $x=1-0.9$ range accessible, both $T_{max}(x)$ and $T_c(x)$ appear to be concave upward, with some uncertainty for the former.

It is not possible to say, given our temperature limitation, what happens between $x=0.5$ and 0.8. Evidently something special occurs in the interval $x=0.4-0.5$ judging from $T_{max}(x)$. Extrapolation of neither $T_{max}(x)$ nor $T_c(x)$ to lower x is possible in principle. However, the rate of variation of these is decreasing as x decreases. It would be remarkable if a line of transitions at temperatures below 1.8 K extends across the diagram in the $x=0.5-0.8$ range.

It seems unlikely that frustration in mixtures in the $x=0.5-0.8$ range is so large as to eliminate a finite-temperature transition. A proposed measure of frustration[36] in systems with predominantly antiferromagnetic interactions is the ratio $|\theta|/T_c$, with θ normally being negative, in $\chi_M = C/(T-\theta)$, for an antiferromagnetic material. For high frustration this ratio is well above unity. In $Co_{1-x}Mn_xCl_2 \cdot H_2O$, $|\theta|/T_c$ ranges from 1.06 to 1.83 from $x=0$ to 0.40 and from 2.27 to 3.08 from $x=1$ to 0.9. However, the present system is not ideal for applying the above criterion. First, there is some lower-dimensional character in both pure systems, and thus one can expect a diminution of T_c on this basis alone. Second, there are predominantly ferromagnetic interactions in $CoCl_2 \cdot H_2O$, leading to a positive θ, despite weaker antiferromagnetic interchain interactions.

Magnetization isotherms for $x=0.30$ exhibited an inflection point that disappeared above 7 K and a hysteresis that was barely detectable above 4.2 K. These features correlate fairly well with those evident in $\chi(T)$: a maximum at 6.25 K and a leveling associated with a transition at 4.8 K. In $x=0.40$ the degree of $M(H)$ curvature is significantly less than in $x=0.30$, as is the hysteresis. A change in the shape of the isotherm is evident between 1.8 and 2.4 K; the curvature is uniform at 4.2 K. These features also correlate well with $\chi(T)$ characteristics, the maximum and transition temperatures in the 2.1–2.0 K region. The magnetization isotherms of $x=0.50$ display only uniform curvature without inflection points, while the hysteresis is rather small. This is consistent with only an incipient maximum in $\chi(T)$ at 1.8 K, with any transition temperature too low to detect.

The nonlinear susceptibility for $x=0.30$ shown in Fig. 10 exhibits obvious structure, including a strong increase below 3.3 K, but no divergence. Attempts to fit the field-cooled magnetization data from which χ_{nl} is obtained, in order to determine $b_3(T)$ and $b_5(T)$ in Eq. (2), led to rather erratic results for these parameters with no sign of divergent behavior. This is not unexpected for a reentrant spin glass. Like $CoCl_2 \cdot H_2O$, the $x=0.30$ mixture should be describable as such, since the 3.3 K upturn, which agrees well with the strong irreversibility temperature for low fields, occurs well below the antiferromagnetic transition near 4.8 K. In $x=0.30$ this transition is much less prominent than in $CoCl_2 \cdot H_2O$. In $CoCl_2 \cdot H_2O$ a similar upturn came in strongly below 5 K, which is also in the region of the strong irreversibility temperature. Clearly visible in Fig. 10 is a local minimum in χ_{nl} near 5 K, close to the antiferromagnetic transition at 4.8 K. Such a feature also occurred for $CoCl_2 \cdot H_2O$ near the 14 K antiferromagnetic transition.

Certain TRM(T) representations shown in Figs. 11–13 display inflection points at 3.41, 2.58, and in the 2.05–2.14 K range for $x=0.30$, 0.40, and 0.50, respectively. These temperatures agree quite well with those plotted in Fig. 5 for the strong irreversibility temperature, in 0.2 kG, vs composition: $T_s = 3.24$, 2.48, and 2.04_4 K for $x=0.30$, 0.40, and 0.50, respectively. For $CoCl_2 \cdot H_2O$ an obvious crossover in the ln M_{TRM} vs T representation occurred near 6.3 K. The T_s value in Fig. 5 for $x=0$ is 6.2_2 K. Thus the ratio $T_s(x)/T_{infl}(x)$ is remarkably uniform, in the range 0.95–0.99, from $x=0$ to 0.50.

The cooling field dependence of the TRM in the mixtures $x=0.30$, 0.40, and 0.50 is much weaker than in $CoCl_2 \cdot H_2O$ and becomes progressively weaker with increasing x. This together with the much more gradual curvature in the magnetization isotherms of even $x=0.30$ compared to those of $CoCl_2 \cdot H_2O$ suggests a progressive reduction in any metamagnetic character, signs of which were present in $CoCl_2 \cdot H_2O$, with increasing x. The development of weaker and more random interchain interactions with mixing is likely to be responsible.

The composition dependences of the TRM noted in Sec. III D 3 reflect the decreases in antiferromagnetic and spin glass transition temperatures with increasing x and the progressive reduction in metamagnetic character. That the 0.5-kG field-cooled TRM values at ~1.85 K for $x=0.30$, 0.40, and 0.50 are larger than the corresponding value in $CoCl_2 \cdot H_2O$ implies even greater irreversibility in the mixtures than in $CoCl_2 \cdot H_2O$. This is also reflected in values of M_{IRR}/H, at 1.9 K and for a 0.2 kG measuring field, as a function of composition; these are 0.016_5, 0.21_2, 0.26_9, and 0.16_9 emu/mol for $x=0$, 0.30, 0.40, and 0.50, respectively. Since M/H has a tendency to increase with increasing x because of the greater fraction of higher-spin manganese ion, it is arguably preferable to refer instead to the value of M_{IRR}/H divided by the field-cooled value of M/H at 1.9 K. Doing so gives the ratios 0.23_9, 0.31_0, 0.31_2, and 0.19_9 in the same order as above. By either measure it appears that irreversible effects are maximized in the $x=0.3-0.4$ region. If for $x=0.30$ the spin glass state should still be described as reentrant, this does not appear to be the case for $x=0.40$ and 0.50.

The temperature dependence of the stretched exponential decay parameters M_0 and τ in Eq. (3) can often be correlated with other properties. Thus the strong increase in the nonlinear susceptibility of $x=0.30$ below 3.3 K has its correspondence in the increase in the TRM below 3.4 K; moreover, an inflection point in certain representations of $M_{TRM}(T)$ occurs at 3.4 K and the strong irreversibility temperature for small fields is also similar (3.35 K for $H=0$). In Fig. 20 it is apparent that $\tau(T)$ for 500-G field-cooled data changes the sense of its temperature variation near 3.4 K, while $\tau(T)$ for the 5 kG field almost certainly does so near the not very different 4.2 K. Earlier estimates were that $M_0(T)$ extrapolates to 0 at 5.5–6 and 4.5–5 K for the 500-G and 5-kG

field-cooled results, respectively. The former temperature range is close to the weak irreversibility temperature of $x=0.30$ for low field. Such a correlation also emerged for $CoCl_2 \cdot H_2O$.[19]

For the $x=0.40$ mixture, the TRM shows a marked increase below about 2.6 K and an inflection in certain $M_{TRM}(T)$ representations also occurs here. It is over temperature ranges including 2.6 K that a change in the sense of variation of τ with T occurs for both the 507 G and 5 kG results. The strong irreversibility temperature for a 0.2 kG field, 2.48 K, is also similar. The extrapolations of $M_0(T)$ to zero value yielded temperature ranges of 4.5–5 and 3.5–4 K for the 507 G and 5 kG TRMs, respectively. It is possible to use $T_w(0)$ values for $x=0$, 0.30, and 0.50 to estimate that $T_w(0)$ for $x=0.40$ is near 5 K. This agrees well with the first of the above extrapolations.

For the $x=0.50$ mixture, the TRM shows a substantial increase below about 2.14 K and an inflection point in certain $M_{TRM}(T)$ representations also occurs here. In temperature ranges rather close ($\sim$0.1 K) to 2.14 K, a change in the sense of variation of $\tau(T)$ is seen for both the 504 G and 5 kG cooling fields. The strong irreversibility temperature for a 0.2 kG field, 2.04_4 K, is also rather similar. Extrapolation of $M_0(T)$ to zero value yielded temperature (ranges) of 2.3_5 and 2.5–3 K for 504 G and 5 kG results, respectively. The latter result is comparable to $T_w(0)$.

The detailed variation of $\tau(T)$ provides at least one unusual feature. The initial decrease in τ with increasing T is expected, since the spin glass should be more frozen at lower temperatures. The change in the sense of variation at somewhat higher temperatures is less expected. If, however, domain size actually grows with increasing temperature in the weak irreversibility regime, then slower relaxation and larger τ should follow.

From Figs. 23–25 it appears that $T\log_{10}(t/\tau_0)$ scaling of the TRM extends through maximum temperatures such that T/T_g ranges from 0.58 to 0.75, where T_g is taken as $T_w(0)=6.75$, 5 (estimate by interpolation), and 3.35 K for $x=0.30$, 0.40, and 0.50, respectively. This is similar to the behavior observed in $CoCl_2 \cdot H_2O$ previously.[19] A failure of such scaling for temperatures above ca. $2T_g/3$ is expected if the assumption of a temperature-independent distribution of barrier heights breaks down as $T \rightarrow T_g^-$.[25] The τ_0 are mostly in the range 10^{-12}–10^{-13} s and significantly smaller than the 10^{-9}–10^{-10} s found for $CoCl_2 \cdot H_2O$. The smaller values here are more similar to those typically found for spin glasses, 10^{-11}–10^{-14} s. Some tendency toward shorter τ_0 for larger x is evident.

Each of the strong irreversibility lines, for $x=0.30$ and 0.50, is characterized by an exponent a, in $\tau_g = ch^a$, slightly below 0.5, with statistical uncertainties of 0.08 or so. Thus these results are in better accordance with the specific prediction for a short-range 3D Ising spin glass [$a=0.53$ (Ref. 30)] than with the mean-field Ising DeAlmeida-Thouless value of 2/3. This was also the case for $CoCl_2 \cdot H_2O$.[19] Since these materials are insulating, and Co^{2+} tends to show considerable single-ion anisotropy and Ising model behavior at low temperatures, this may be significant. However, observation of a merely effective exponent influenced by reduced temperature limitations cannot be ruled out.[37]

The prefactor in the theoretical form $\tau_g \propto h^{0.53}$ has not been given. The values of c for the strong irreversibility lines of $x=0.30$ and 0.50 are $c=0.23_2$ and 0.17_9, respectively, where the fitted exponents are 0.47 and 0.49 in the same order. For the model curve in Fig. 28, assuming $a=0.53$, the prefactor c is 0.25_1, rather similar to 0.23_2 above. The original DeAlmeida-Thouless form for the Ising spin glass is usually written $\tau_g^3=(3/4)h^2$; this may be recast as $\tau_g = 0.90_9 h^{2/3}$. In the mean-field treatment of the isotropic m-component spin glass, the freezing of longitudinal components (strong irreversibility line) is of the form $\tau_{cr}^3=[(m+1)(m+2)/8]h^2$; a crossover line rather than one of true phase transitions occurs. For $m=3$ this becomes $\tau_{cr}^3 = (20/8)h^2$ or $\tau_{cr}=1.36h^{2/3}$. For an m-component spin glass with sufficiently strong anisotropy, a DeAlmeida-Thouless-like line is again predicted and is the only irreversibility line: $\tau_g^3=[(m+2)/4m]h^2$. For $m=3$ this becomes $\tau_g^3 = (5/12)h^2$ or $\tau_g = 0.74_7 h^{2/3}$. Experimental prefactors rarely agree well with theoretical ones, and we are not invoking these mean-field predictions for our results, but that the prefactors determined here are similar in magnitude is a favorable sign. In fitting the strong irreversibility line in $CoCl_2 \cdot H_2O$ to the theoretical form $\tau_g \propto h^{0.53}$, a rather larger prefactor of 4.2_3 was obtained.

In certain respects the weak irreversibility lines for $x=0.30$ and 0.50 are even more interesting. In contrast to that found for $CoCl_2 \cdot H_2O$,[19] they show substantial field dependence. The scatter in $T_w(H)$ values is obviously such as to make any fits uncertain, and the values of the exponents in $\tau_g = ch^a$, $a=0.66$ and 0.43 for $x=0.30$ and 0.50, respectively, differ substantially, as do the prefactors 2.0_8 and 0.68_8. But the form of these lines is very different from the Gabay-Toulouse line of an m-component spin glass where the transverse spin components freeze: $\tau_g=[(m^2+4m+2)/4(m+2)^2]h^2$, which for $m=3$ becomes $\tau_g = (23/100)h^2$.

An explanation of this behavior may reside in the existence of strong random anisotropy in $Co_{1-x}Mn_xCl_2 \cdot H_2O$. Mean-field theory for vector spin glasses with anisotropy defines the strong anisotropy regime as that for which $d \gg h^{2/3}$. Here d is an anisotropy parameter defined as the ratio of the mean anisotropy strength and the mean exchange strength, i.e., $d=D/J$.[33] For sufficiently strong random anisotropy, the low-field portion of the Gabay-Toulouse upper (weak) irreversibility line becomes Ising-like, according to $h^2 = 4\tau_g^3/(m+2)$.[38] This can be recast for $m=3$ as $\tau_g = 1.07_7 h^{2/3}$. A crossover in the form of this line to standard Gabay-Toulouse type is predicted to occur, but is pushed to higher fields as the mean exchange interaction becomes small and as D becomes much bigger than J. It is difficult to estimate d precisely; for $CoCl_2 \cdot H_2O$, a value of about 0.005 was obtained based on the dipolar interaction as the origin of the anisotropy. Other possible sources are antisymmetric exchange and single-ion anisotropy. In $CoCl_2 \cdot H_2O$ it is unlikely that the strong anisotropy case occurs and two irreversibility lines were observed. In $Co_{1-x}Mn_xCl_2 \cdot H_2O$ the mean exchange interaction is smaller than in $CoCl_2 \cdot H_2O$, as evidenced by the variations in θ and T_c with x, both of which become quite small in the $x=0.5$–0.6 region. Moreover, randomness in the anisotropy may be induced by mixing. Al-

though the weak irreversibility exponents are not very precisely determined, they are obviously much lower than 2 and much closer to the value 2/3.

Investigation of the present mixed system by other techniques is called for. Frequency-dependent susceptibility measurements could provide valuable information on the nature of the observed transitions. NMR measurements, and of course neutron scattering, could provide a detailed understanding of the microscopic spin state as a function of temperature. In order to explore the composition range from 0.5 to 0.8, somewhat lower temperatures than 1.8 K are also needed.

ACKNOWLEDGMENTS

This work was supported by National Science Foundation, Solid State Chemistry, Grant No. DMR-9527357, and by the Petroleum Research Fund of the American Chemical Society.

*Present address: Chemistry Department, Yale University, New Haven, CT 06520.

[1] S. Fishman and A. Aharony, Phys. Rev. B **18**, 3507 (1978).
[2] D. Mukamel, Phys. Rev. Lett. **46**, 845 (1981).
[3] P.-Z. Wong, Phys. Rev. B **34**, 1864 (1986); P.-Z. Wong, P. M. Horn, R. J. Birgeneau, and G. Shirane, *ibid.* **27**, 428 (1983).
[4] W. Nitsche and W. Kleeman, J. Magn. Magn. Mater. **54–57**, 37 (1986); Phys. Rev. B **36**, 8587 (1987); B. D. Howes, D. C. Price, and M. C. K. Wiltshire, J. Phys. C **17**, 3669 (1984).
[5] K. Katsumata, S. M. Shapiro, M. Matsuda, G. Shirane, and J. Tuchendler, Phys. Rev. B **46**, 14 906 (1992).
[6] G. C. DeFotis, C. Pohl, S. A. Pugh, and E. Sinn, J. Chem. Phys. **80**, 2079 (1984).
[7] K. Katsumata, M. Kobayashi, T. Sato, and Y. Miyako, Phys. Rev. B **19**, 2700 (1979); M. Kobayashi, K. Katsumata, T. Sato, and Y. Miyako, J. Phys. Soc. Jpn. **46**, 1467 (1979); K. Katsumata, M. Kobayashi, and H. Yoshizawa, Phys. Rev. Lett. **43**, 960 (1979).
[8] S. Fishman and A. Aharony, Phys. Rev. B **19**, 3776 (1979); **21**, 280 (1980).
[9] H. A. Katori and A. Ito, J. Phys. Soc. Jpn. **62**, 4488 (1993), and references therein.
[10] G. C. DeFotis, D. S. Mantus, E. M. McGhee, K. R. Echols, and R. S. Wiese, Phys. Rev. B **38**, 11 486 (1988); G. C. DeFotis and E. D. Remy, J. Phys. (Paris), Colloq. **49**, C8-1053 (1988); G. C. DeFotis and K. D. Dell, Phys. Rev. B **50**, 9937 (1994).
[11] K. Zenmyo and H. Kubo, J. Phys. Soc. Jpn. **64**, 1320 (1995); H. Kubo, K. Zenmyo, and T. Kato, *ibid.* **65**, 4045 (1996), and references therein.
[12] B. Morosin and E. J. Graeber, Acta Crystallogr. **16**, 1176 (1963); J. Chem. Phys. **42**, 898 (1965).
[13] G. C. DeFotis, R. S. Wiese, and C. W. Scherrer, J. Appl. Phys. **67**, 5857 (1990).
[14] J. A. Lukin, S. A. Friedberg, and G. C. DeFotis, J. Appl. Phys. **69**, 5807 (1991).
[15] J. N. McElearney, S. Merchant, and R. L. Carlin, Inorg. Chem. **12**, 906 (1973).
[16] G. C. DeFotis, R. V. Chamberlain, W. R. A. Jarvis, and D. J. Krovich, J. Magn. Magn. Mater. **104–107**, 1603 (1992).
[17] A. Narath, Phys. Rev. **136**, A766 (1964).
[18] J. A. Lukin, S. A. Friedberg, S. Chandarlapaty, W. W. Brubaker, C. C. Cinquina, and G. C. DeFotis, J. Appl. Phys. **75**, 5529 (1994).
[19] G. C. DeFotis, G. A. Coffey, C. C. Cinquina, S. Chandarlapaty, W. W. Brubaker, D. J. Krovich, R. V. Chamberlain, and W. R. A. Jarvis, Phys. Rev. B **51**, 15 113 (1995).
[20] T. Oguchi, J. Phys. Soc. Jpn. **20**, 2236 (1965).
[21] J. B. Torrance and M. Tinkham, Phys. Rev. **187**, 595 (1969).
[22] J. D. Hanawalt, H. W. Rinn, and L. K. Frevel, Anal. Chem. **10**, 457 (1938).
[23] I. Bkouche-Waksman, C. R. Seances Acad. Sci., Ser. C **271**, 581 (1970).
[24] M. E. Fisher, Philos. Mag. **7**, 1731 (1962).
[25] R. Omari, J. J. Prejean, and J. Souletie, J. Phys. (Paris) **45**, 1809 (1984).
[26] G. Parisi and F. Ritort, J. Phys. I **3**, 969 (1993).
[27] A. Labarta, O. Iglessias, L. Balcells, and F. Badia, Phys. Rev. B **48**, 10 240 (1993).
[28] E. Vincent, J. Hammann, P. Prene, and E. Tronc, J. Phys. I **4**, 273 (1994).
[29] G. G. Kenning, D. Chu, and R. Orbach, Phys. Rev. Lett. **66**, 2923 (1991).
[30] F. Ritort, Phys. Rev. B **50**, 6844 (1994).
[31] J. R. L. De Almeida and D. J. Thouless, J. Phys. A **11**, 983 (1978).
[32] M. Gabay and G. Toulouse, Phys. Rev. Lett. **47**, 201 (1981).
[33] G. Kotliar and H. Sompolinsky, Phys. Rev. Lett. **53**, 1751 (1984).
[34] F. Lefloch, J. Hammann, M. Ocio, and E. Vincent, Physica B **203**, 63 (1994).
[35] F. Bernardot and C. Rigaux, Phys. Rev. B **56**, 2328 (1997).
[36] A. P. Ramirez, J. Appl. Phys. **70**, 5952 (1991); Annu. Rev. Mater. Sci. **24**, 453 (1994).
[37] A. Zieba and Z. Lodziana, Phase Transit. **57**, 161 (1996).
[38] K. H. Fischer, Z. Phys. B **60**, 151 (1985).